Title: Square Grid Metal-Chloranilate Networks as Robust Host Systems for Guest Sorption

Authors: Brendan Francis Abrahams; Christopher J. Kingsbury; Josie E. Auckett; Hubert Chevreau; A. David Dharma; Samuel Duyker; Qilin He; Carol Hua; Timothy A. Hudson; Keith S. Murray; Wasinee Phonsri; Vanessa K. Peterson; Richard Robson; Keith F. White

To be cited as: 10.1002/chem.201805600

Link to VoR: https://doi.org/10.1002/chem.201805600

Square Grid Metal-Chloranilate Networks as Robust Host Systems for Guest Sorption

Christopher J. Kingsbury,[a] Brendan F. Abrahams,*[a] Josie E. Auckett,[b], Hubert Chevreau[b], A. David Dharma,[a] Samuel Duyker[b], Qilin He,[c] Carol Hua,[a,c] Timothy A. Hudson,[a] Keith S. Murray,[d] Wasinee Phonsri,[d]Vanessa K. Peterson,[b] Richard Robson,*[a] Keith F. White[a,e]

[a] *C. J. Kingsbury, A/Prof. B. F. Abrahams, A. D. Dharma, Dr C. Hua, Dr T. A. Hudson, Prof. R. Robson, Dr K. F. White*
School of Chemistry, University of Melbourne, Parkville, Victoria 3010 (Australia)

[b] *Dr J. E. Auckett, Prof. V. K. Peterson, Dr S. Duyker, Dr H. Chevreau*
Australian Centre for Neutron Scattering, Australian Nuclear Science and Technology Organisation, New South Wales 2234 (Australia)

[c] *Dr C. Hua, Q. He*
Department of Chemistry, Northwestern University, Evanston, Illinois 60208-3113, (USA)

[d] *Emeritus Prof. K. S. Murray, Dr W. Phonsri*
School of Chemistry, Monash University, Clayton, Victoria 3800 (Australia)

[e] *Dr K. F. White*
La Trobe Institute of Molecular Sciences, La Trobe University, Albury-Wodonga, Australia

Abstract

Reaction of the chloranilate dianion with $Y(NO_3)_3$ in the presence of Et_4N^+ in the appropriate proportions results in the formation of $(Et_4N)[Y(can)_2]$, which consists of anionic square-grid coordination polymer sheets with interleaved layers of counter-cations. These counter-cations, which serve as squat pillars between $[Y(can)_2]$ sheets lead to alignment of the square grid sheets and the subsequent generation of square channels running perpendicular to the sheets. The crystals are found to be porous and retain crystallinity following cycles of adsorption and desorption. This compound exhibits a high affinity for volatile guest molecules, which could be identified within the framework by crystallographic methods. *In situ* neutron powder diffraction indicates a size-shape complementarity leading to a strong interaction between host and guest for CO_2 and CH_4. Single crystal X-ray diffraction experiments indicates significant interactions between the host framework and discrete I_2 or Br_2 molecules. A series of isostructural compounds $(cat)[M^{III}(X\text{-}an)_2]$ with M = Sc, Gd, Tb, Dy, Ho, Er, Yb, Lu, Bi or In, cat = Et_4N, Me_4N and X-an = chloranilate, bromanilate or cyanochloranilate bridging ligands have been generated. The magnetic properties of representative examples $(Et_4N)[Gd(can)_2]$ and $(Et_4N)[Dy(can)_2]$ are reported with normal DC susceptibility but unusual AC susceptibility data noted for $(Et_4N)[Gd(can)_2]$.

Introduction

Investigations of coordination polymers in the early 1990s commonly focussed on the use of bridging pyridyl-based ligands, such as 4,4'-bipyridine, to create open-type structures in which metal centres serve as nodes.[1] Whilst the generation of these materials succeeded in demonstrating the potential of a net-based approach to the design of coordination networks, these types of materials were, in general, not particularly robust. The employment of bridging ligands which are charged or contain chelating groups offers the prospect of forming stable networks that exhibit microporosity.

The dianion of 2,5-dihydroxybenzoquinone (H_2dhbq, **I**, X = H) contains both chelating and charged metal binding groups and has been used in the generation of a wide variety of coordination polymers, from chains to 2D and 3D networks.[2] As a consequence of its chelating groups and negative charge, it binds strongly and predictably to metal centres to yield robust structures.[3] Commonly, the coordination polymers generated from the combination of dhbq anions and divalent metals are anionic. For example, when octahedral Mn(II) centres are bridged by $dhbq^{2-}$ ligands, a 2D anionic hexagonal network of composition $[Mn_2(dhbq)_3]^{2-}$ is formed with Na^+ ions providing the charge balance.[4] The connectivity of the network has been found to be very sensitive to the nature of the cation. When tetrabutylammonium (NBu_4^+) is used as a countercation, the octahedral Mn(II) centres are still linked by three bridging $dhbq^{2-}$ anions but a 3D network with the (10,3)*a* topology is obtained, clearly indicating that the countercation can play a significant structure-directing role.[3a] Similar structural behavior is apparent when related ligands such as chloranilate (**I**, X = Cl) are employed.[5]

In addition to providing strong, predictable links between metal centres, interest in dhbq-type ligands relates to the accessibility of multiple oxidation states. The quinone form (**I**) is capable of undergoing a 2-electron reduction to the aromatic form (**III**). Under certain circumstances an intermediate -3 radical form (**II**) can also be identified.[6] The ability of the bridging ligand to exist in multiple oxidation states therefore offers the prospect of forming redox-active networks.

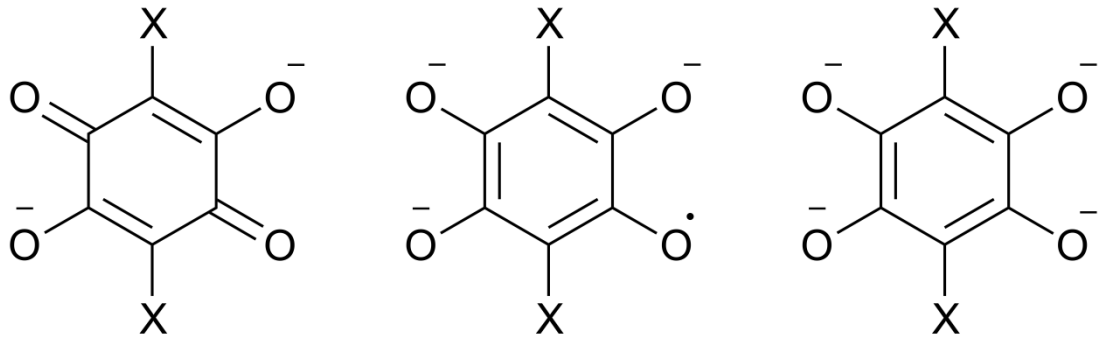

I **II** **III**

Another advantage of the dhbq-type ligand is the possibility to introduce a range of different substituents at the 3,6 positions, e.g. X = F, Cl, Br, I, NO_2, CN, CH_3 etc. thus allowing the physical and chemical properties of the ligand to be modified. These groups at the 3 and 6 positions not only affect the donor strength of the ligand but also impact upon the reduction potential of the ligand. The most widely studied ligands in this system are the dianions of dihydroxybenzoquinone (H_2dhbq, **I**, X = H) and chloranilic acid (H_2can, **I**, X = Cl).

In 2011 we reported a chiral, square grid anionic framework structure of composition $[Sn^{IV}Ca^{II}(can)_4]^{2-}$ in which 8-coordinate Sn(IV) and Ca(II) centres are bridged by chelating chloranilate ligands.[7] Parallel square grid sheets are aligned with each other in a manner that produces open square channels perpendicular to the plane of the 2D network. The Et_4N^+ cation plays a similar role in this structure as it does in the aforementioned $[M_2(can)_3]^{2-}$ networks which have hexagonal channels.[5a] The resulting material was shown to be porous. Lanthanoids are known to form 6,3-networks with dhbq-related ligands, in which each metal centre is bound to three dhbq-type bridging, and co-ligands such as water complete the coordination sphere to give coordination numbers of 8 or 9.[8] In 2002 we had shown that that it was possible to bridge 8-coordinate Y(III) centres by chloranilate ligands within a diamond-like network[8b] and recently, Gomez-Garcia and co-workers reported the formation of a square grid network of composition $(H_3O)[Dy(C_6O_4(CN)Cl)_2(H_2O)]\cdot 4H_2O$ in which each Dy(III) center is linked to four other Dy centers by chelating/bridging chlorocyanilate ligands.[9] A water molecule completes a 9-coordinate

geometry around each Dy center. The $[Dy(C_6O_4(CN)Cl)_2(H_2O)]$ square grid network is slightly undulating and has a lower symmetry (monoclinic) than that of the Sn-Ca network. It was of interest to determine if +3 lanthanoids or pseudo-lanthanoids such as Y^{III} could play a structural role similar to that of the 8-coordinate Sn^{IV} and Ca^{II} metal ions in forming a tetragonal structure in which tetraethylammonium cation serves as pillars between anionic sheets. In addition to the lanthanoid elements, the investigation was extended to include trivalent main-group element cations such as In^{III} and Bi^{III}.

Herein we describe the synthesis and crystal structures of a series of 2D anionic networks in which a variety of relatively large +3 metal ions serve as 4-connecting nodes linked by chloranilate or other related dhbq-type ligands. A description of the host behaviour of these materials is also presented with a particular emphasis on determining the location of guest molecules within the pores. DC and AC magnetic studies on on the paramagnetic compounds $(Et_4N)[Gd(can)_2]$ and $(Et_4N)[Dy(can)_2]$ are also described.

Results and discussion

Synthesis and Crystal Structure Analyses of $[M^{III}(can)_2]^-$ Networks

In the formation of network materials involving dhbq-related ligands it has been found that the slow generation of the bridging ligand either by hydrolysis of diamino-benzoquinone or oxidation of tetrahydroxy-benzene is a synthetic approach that often produces high purity crystalline products.[3a, 3b, 5a, 10] In this current work, single crystals of the chloranilate networks have been generated using H_4can, the tetraprotonated form of **III** (X = Cl), as a starting material. Aerial oxidation of H_4can in the reaction mixture leads to a slow and steady generation of the chloranilate dianion in a process that aids the formation of good quality crystals. In the case of the dianionic bridging ligands, Bran (**I**, X = Br, bromanilate) and ClCNan (**I**, X = Cl in one position and X = CN at the other, chlorocyanilate) a similar slow oxidation process of H_4Bran and H_4ClCNan respectively is employed.

The acetone solvate of $(Et_4N)[Y(can)_2]$ was synthesised by dissolving H_4can and lithium acetate in acetone and carefully layering this above an aqueous solution of tetraethylammonium bromide and yttrium nitrate. Slow mixing of the two solutions led to the formation, over a period of a week, of very dark purple, square block-shaped crystals of composition $(Et_4N)[Y(can)_2]$. A similar synthetic approach was employed in the synthesis of $(Et_4N)[M(can)_2]$ (M = Sc, Gd, Tb, Dy, Ho, Er, Yb, Lu, In and Bi), $(Et_4N)[Bi(Bran)_2]$ and $(Et_4N)[Bi(ClCNan)_2]$. When Sc^{III} is used it is possible to obtain a similar structure with tetramethylammonium in place of tetraethylammonium to form a compound of composition $(Me_4N)[Sc(can)_2]$. All of these compounds formed as acetone solvates.

Single crystal X-ray structural analysis of $(Et_4N)[Y(can)_2]\cdot(CH_3)_2CO$ revealed a tetragonal unit cell with the adoption of the space group *I*4/*mcm*. The structure determination indicated a 2D anionic square grid network (Figure 1a). The mean plane of the anionic network is normal to the *c*-axis. Each Y^{III} centre, which is located on a site of symmetry 422, is coordinated by four chelating can^{2-} ligands which bridge to four equivalent Y^{III} centres. Structural data are presented in Table 1. The coordination geometry may be described as a square anti-prism with the ligands adopting a "propeller-type" arrangement around the metal centre with either Λ or Δ configuration. Within a single sheet, every Y^{III} centre with a Λ configuration is linked via can^{2-} ligands to four Y^{III} centres with a Δ configuration and vice versa. Thus, each sheet consists of a racemic mixture of Λ and Δ centres. Each can^{2-} ligand is centered on a site of 2/*m* symmetry.

The $[Y(can)_2]^-$ anionic sheets stack in a manner which generates square channels parallel to the *c*-axis as indicated in Figure 1b. Tetraethylammonium cations lie halfway between pairs of Y^{III} centres belonging to adjacent parallel sheets with the nitrogen atom located on a site of 4/*m* symmetry. The tetraethylammonium cation is disordered over a pair of symmetry-related sites, with each of the eight methylene hydrogen atoms participating in a C–H···O hydrogen bond that extends to a coordinated oxygen atom as shown in Figure 1c. Charge assisted C–H···O hydrogen bonds result in the alignment of the sheets and allow the tetraethylammonium cation to serve as a type of pillar in the 3D structure. The separation between Y^{III} centres of adjacent sheets corresponds to half the *c* cell length. Interestingly, the tetraethylammonium cation plays a similar role in the 6,3- structures, where the cation fits neatly into an

octahedral cavity formed by three Cl atoms from the sheet above and three from the sheet below.[5a] In the case of $(Et_4N)[Y(can)_2]$ the tetraethylammonium cation fits snugly into the cavity defined by the eight chlorine atoms which are at the vertices of a distorted square prism. The interaction of the cation with the $[Y(can)_2]^{2-}$ anionic networks not only results in the alignment of the Y centres but also leads to an alternation in the configuration of the Y centres along a direction parallel to the *c*-axis i.e. Λ···Δ···Λ···Δ···Λ···Δ as is apparent from inspection of Figure 1c. The structure is in fact similar to the aforementioned $(Et_4N)_2[SnCa(can)_4]$.[7] In contrast to the Y^{III} structure, the alternation of Sn^{IV} and Ca^{II} centres results in a chiral crystal.

a)

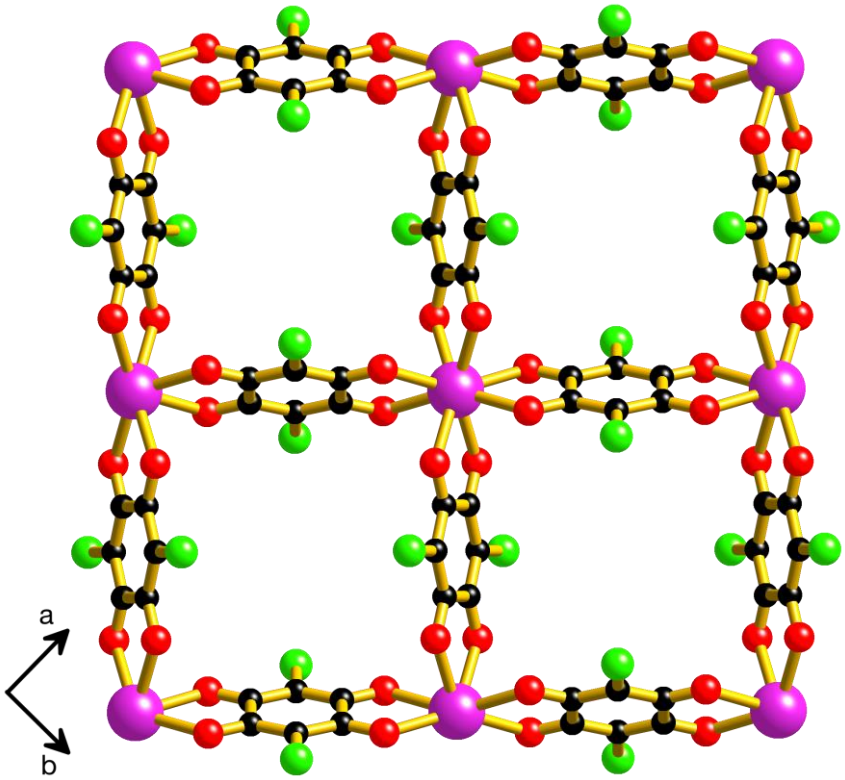

b)

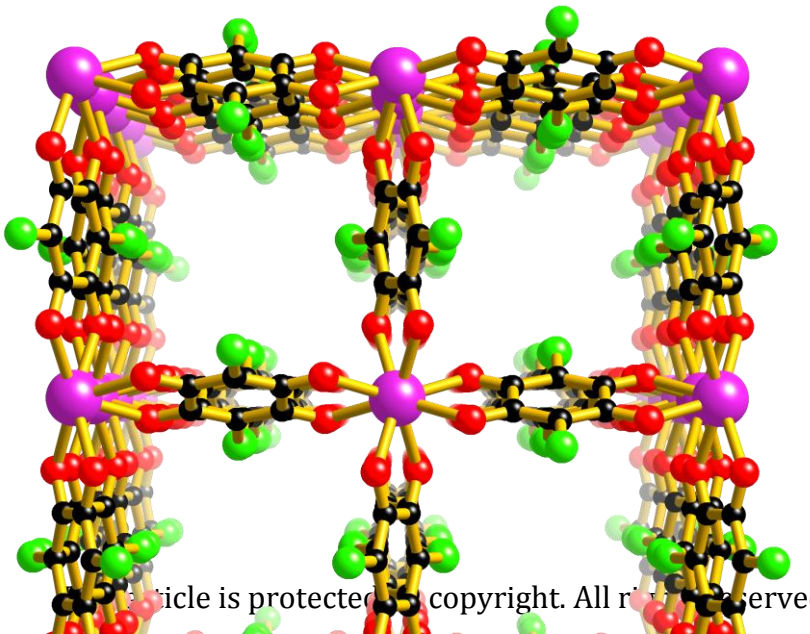

c)

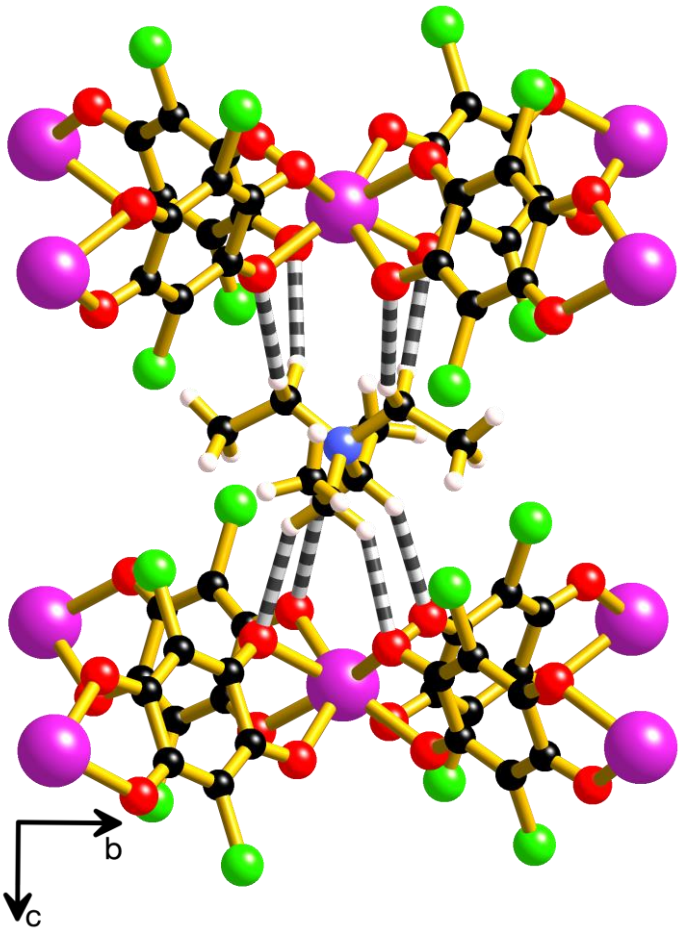

Figure 1. The crystal structure of $(Et_4N)[Y(can)_2]$ showing a) a section of the square grid $[Y(can)_2]^-$ anionic framework, b) the alignment of $[Y(can)_2]^-$ sheets to produce square channels perpendicular to the plane of the sheets; cations have been omitted from this image and c) the location of the tetraethylammonium between Y centres of adjacent sheets; striped connections indicate C–H···O hydrogen bonds Colour code: C black, N blue, O red, Cl green, Y pink.

If the crystal is transferred directly from the mother liquor to a protective oil before being placed on the diffractometer at 130 K then electron density consistent with disordered acetone is apparent in the square holes of the networks. The disordered solvent was treated using the SQUEEZE routine within PLATON[11] which indicated that ~25% of the crystal volume was available for guest uptake. This approximates to ~190 $Å^3$ of guest accessible space per Y centre.

An additional single crystal structure of $(Et_4N)[Y(can)_2]$ was determined at 375 K which showed the same 4,4- network structure with open channels devoid of acetone.

Single crystal structure determinations of the acetone solvates of $(Et_4N)[M(can)_2]$ (M = Sc, Gd, Tb, Dy, Ho, Er, Yb, Lu, In and Bi) reveal essentially the same type of structure with the adoption of similar cell dimensions as well as the same space group, *I*4/*mcm*. The separation between metal centres bridged by a chloranilate ligand ranges from 8.2802(3) Å for $(Et_4N)[Sc(can)_2]$ to 8.7120(3) Å for $(Et_4N)[Bi(can)_2]$ (Table 1). The variation in intra-sheet M···M separations can be rationalised in terms of the size of the trivalent metal cations. Inter-sheet M···M separations show much less variation and there is no clear relationship between the size of the metal ion and the separation of the sheets. The M···M separation varies from 10.0539(3) Å for $(Et_4N)[Gd(can)_2]$ to 10.3349(2) Å for $(Et_4N)[Ho(can)_2]$. Across the series of compounds considered so far, inclination of the chloranilate ligand to the stacking direction (parallel to the *c*- axis) varies from 18.5 - 26.4° (see Table 1). The crystal structure analyses indicate between one and two acetone molecules per metal centre. The fraction of the crystal volume unoccupied by the $(Et_4N)[M(can)_2]$ framework ranges from 23.2 % for $(Et_4N)[Sc(can)_2]$ to 27.0 % for $(Et_4N)[Ho(can)_2]$.

$(Et_4N)[Bi(Bran)_2]$ and $(Et_4N)[Bi(ClCNan)_2]$

The generation of the same square grid metal chloranilate structure with a range of metal centres suggested a broad structural tolerance with respect to the size and nature of the trivalent metal ion that can be accommodated in this type of coordination polymer. It was thus of interest to determine if the use of other anilate ligands would also yield the same structural type or indeed whether the generation of the structure was restricted to chloranilate as the bridging ligand. The combination of Bi^{III} and $Bran^{2-}$ in the presence of Et_4N^+ led to the formation of $(Et_4N)[Bi(Bran)_2]$. The structure of the anionic network closely resembles the chloranilate structure. Inspection of geometrical data presented in Table 1 reveal that the separation between ligand-bridged Bi^{III} centres is ~0.08 Å longer in the bromanilate case. The separation between the sheets is ~0.2 Å greater than in the chloranilate analogue.

A similar structure to $(Et_4N)[Bi(can)_2]$ is obtained when chlorocyanilate (ClCNan) is employed as the bridging ligand to yield $(Et_4N)[Bi(ClCNan)_2]$. This is perhaps unsurprising given that $ClCNan^{2-}$ differs from can^{2-} only with respect to the substitution of one of the chlorine atoms for a cyano group. Within the

structure the cyano and chloro groups are disordered. Inspection of Table 1 reveal only minor differences in structural parameters between $(Et_4N)[Bi(can)_2]$ and $(Et_4N)[Bi(ClCNan)_2]$.

$(Me_4N)[Sc(can)_2]$

A satisfactory crystal structure determination of $(Me_4N)[Sc(can)_2]$, in its solvated form, could not be obtained. However, when data were collected at a temperature high enough to remove the solvent molecules, the structure could be determined. The crystal structure analysis showed an anionic coordination polymer similar in structure and connectivity to that of $(Et_4N)[Y(can)_2]$ with the adoption of the same space group, *I*4/*mcm*. The inter-sheet length (corresponding to half the length of the *c* axis) is the shortest of the compounds considered here, presumably due to the incorporation of the smaller Me_4N^+ cation instead of Et_4N^+ and the incorporation of the relatively small Sc(III) centres. The Me_4N^+ cations lie above and below the Sc centres and participate in C–H···O interactions with coordinated oxygen atoms. These charge-assisted hydrogen bonds are similar to those found for the tetraethylammonium cation structures described above.

Table 1. Geometrical data obtained from single crystal structure determinations of $[M(anilate)_2]^-$ network structures. All data collected at 130 K unless otherwise indicated.

Compound	**Intrasheet M-M separation (Å)**	**Intersheet M-M separation (Å)**	**Anilate inclination to *c* axis (degrees)**	**Calc.* void volume (%)**
$(Et_4N)[Y(can)_2]\cdot(CH_3)_2CO$	8.57861(14)	10.1285(2)	23.178(12)	24.9
$(Et_4N)[Sc(can)_2]\cdot(CH_3)_2CO$	8.2802(3)	10.2009(9)	26.43(4)	22.7
$(Et_4N)[In(can)_2]\cdot1.5(CH_3)_2CO$	8.3564(2)	10.3805(4)	21.04(3)	24.0
$(Et_4N)[Gd(can)_2]\cdot(CH_3)_2CO$	8.66368(14)	10.0539(3)	23.78(2)	25.3
$(Et_4N)[Tb(can)_2]\cdot1.5(CH_3)_2CO$	8.63207(14)	10.1176(3)	22.36(3)	25.4
$(Et_4N)[Dy(can)_2]\cdot1.5(CH_3)_2CO$	8.6195(2)	10.245(6)	20.03(3)	26.6
$(Et_4N)[Ho(can)_2]\cdot1.5(CH_3)_2CO)$	8.59764(14)	10.3349(2)	18.473(19)	26.9
$(Et_4N)[Er(can)_2]\cdot(CH_3)_2CO$	8.55005(14)	10.1101(2)	23.974(18)	24.7
$(Et_4N)[Yb(can)_2]\cdot(CH_3)_2CO$ (280 K)	8.5226(2)	10.2479(6)	22.86(3)	25.0
$(Et_4N)[Lu(can)_2]\cdot1.5(CH_3)_2CO$	8.5006(2)	10.2632(4)	20.41(3)	25.4
$(Et_4N)[Bi(can)_2]\cdot2(CH_3)_2CO$ (293 K)	8.7120(3)	10.2040(9)	18.88(5)	27.4
$(Et_4N)[Bi(Bran)_2]\cdot1.5(CH_3)_2CO$	8.79499(14)	10.4054(2)	17.734(9)	27.9
$(Et_4N)[Bi(ClCNan)_2]\cdot1.5(CH_3)_2CO$	8.7336(2)	10.2769(4)	20.2(3)	28.5
$(Me_4N)[Sc(can)_2]$ (400 K)	8.26480(14)	10.0185(3)	27.56(5)	31.1
$(Et_4N)[Y(can)_2]\cdot0.91Br_2$	8.5808(9)	10.157(1)	23.55(5)	-
$(Et_4N)[Y(can)_2]\cdot1.87I_2$	8.6090(2)	10.4318(7)	14.84(5)	-
$(Et_4N)[Y(can)_2]\cdot1.43CS_2$	8.5979(2)	10.1927(4)	20.998(18)	-
$(Et_4N)[Y(can)_2]$ (375 K)	8.5819(2)	10.1465(5)	27.14(9)	25.9

* Calculated volume of solvent filled voids using the Mercury program Voids tool, with 0.2 Å grid spacing and a probe radius of 1.2 Å.

Thermogravimetric analysis

Thermogravimetric analysis (TGA) of the representative compounds $(Et_4N)[M(can)_2]$ (M = Y, Tb, Ho, Er, Yb) and $(Me_4N)[Sc(can)_2]$ showed the samples were stable up to 380 °C, after which, decomposition occurs (S7, Supporting Information).

In all of the structures discussed above, the loss of acetone occurs under ambient conditions with retention of single crystal character. The existence of channels and retention of the crystalline structure upon desolvation, along with the thermal stability of the materials, as indicated by TGA, suggested that this family of compounds could potentially serve as host systems for suitably sized guest molecules. The

following sections describe investigations of the ability of $(Et_4N)[Y(can)_2]$, as a representative compound, to serve as a host material. These investigations employed both manometric and diffraction techniques.

Host behavior of $(Et_4N)[Y(can)_2]$

The vast majority of porosity studies on coordination polymers have involved investigations of neutral rather than charged networks. This is because of understandable concerns by researchers that counterions will either block channels or occupy pore space within the framework, thereby reducing the space available for guest molecules. In the type of structure presented here the countercation does not occupy pore space but rather plays a key structural role in which it may be considered to act as a pillar. By separating the 2D sheets the countercation actually serves to increase the inter-framework void space rather than being an obstruction.

This exploration of the host properties of $(Et_4N)[Y(can)_2]$ is divided into three sections. The first section involves single crystal structure determination of compounds in which the guest molecules CS_2, I_2 and Br_2 have been incorporated into the square channels. The second section is focussed on gas adsorption, in particular, the adsorption of H_2, N_2, CH_4 and CO_2 using manometric techniques. The final section, examining the host properties of these materials, is concerned with a detailed structural investigation of the H_2, CO_2 and CH_4 uptake employing powder neutron diffraction. In particular, this investigation is directed towards identifying the location of the guests in the channel and the order in which various sites are filled by the guest molecules.

Single crystal structural analysis of $(Et_4N)[Y(can)_2]$ with interstitial guest molecules

$(Et_4N)[Y(can)_2]\cdot\sim1.4\ (CS_2)$

When single crystals of the desolvated material, $(Et_4N)[Y(can)_2]$ are immersed in liquid CS_2 in a capped vial and left for 24 hours, CS_2 is incorporated into the crystalline material. A single crystal structure determination revealed similar cell dimensions to that found for the acetone solvate. Peaks of electron density consistent with the incorporation of CS_2 into the channels of the crystal were clearly apparent.

The CS_2 molecules are disordered over many positions with two distinct types of interaction with the host network apparent. The parallel-to-sheet (site 1) arrangement shown in Figure 2a allows for two CS_2 molecules to be accommodated in a single '$Y_4(can)_4$ square'. The closest contact between CS_2 molecules is between C atoms with a separation of 3.54 Å which is a little longer the sum of the van der Waals radii (3.4 Å).[12] It is estimated that approximately half of the squares are occupied by CS_2 in this manner. Of particular note is the relatively close contact of 3.30 Å between a sulfur atom and a chloranilate carbon atom bound to the Cl, which is shorter than the sum of the van der Waals radii for these two atoms of 3.50 Å.[12] Almost all of the remaining $Y_4(can)_4$ squares contain only a single CS_2 molecule, disordered over eight symmetry-related positions (site 2); four of these orientations are shown in Figure 2b. The total sum of CS_2 molecules per square cavity, as indicated by refinement of site occupancies, is 1.43(4).

a)

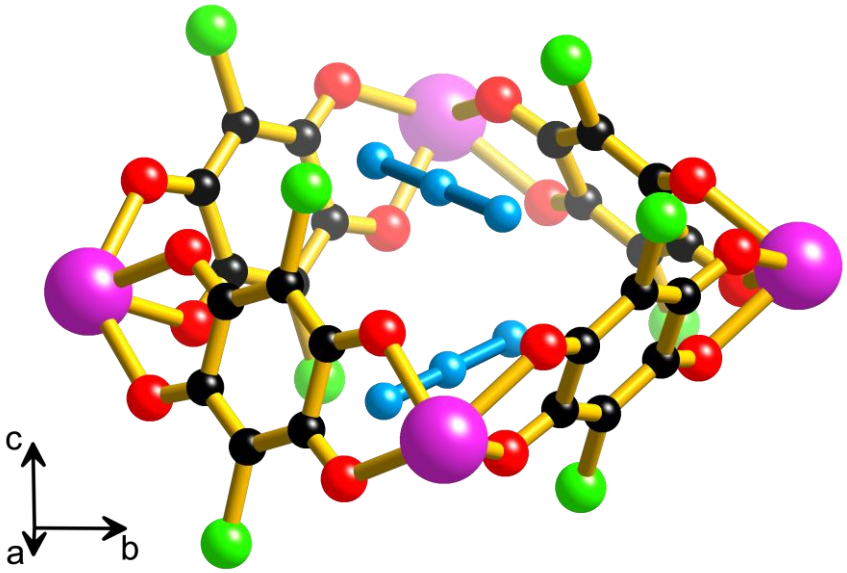

b)

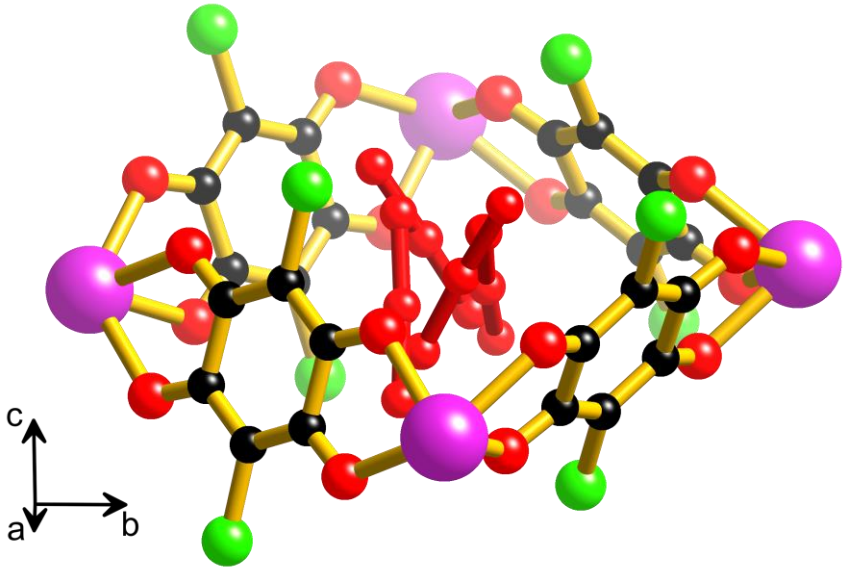

Figure 2. Square cavities within the $[Y(can)_2]^-$ framework occupied by CS_2 molecules showing a) the two site 1 locations of the CS_2 molecules (blue); each orientation has 50% occupancy and b) four of the eight equivalent site 2 locations of CS_2 (red); each of the locations has ~5% occupancy.

$(Et_4N)[Y(can)_2]\cdot 1.9(I_2)$

Single crystals of the desolvated material $(Et_4N)[Y(can)_2]$ were placed in a capped vial containing solid I_2, and left for two days. During this time, vapor diffusion of the iodine into the square channels of the host occurred to generate a compound of composition, $(Et_4N)[Y(can)_2]\cdot 1.9(I_2)$. As with the CS_2 solvate, the host structure is maintained upon inclusion of the guest, as indicated by single crystal X-ray diffraction. Iodine molecules were clearly apparent in the square cavities and occupied positions corresponding to that of the dominant site 1 location for the CS_2 in $(Et_4N)[Y(can)_2]\cdot 1.43(CS_2)$. Refinement of the site occupancies for the iodine atoms indicated 1.872(14) I_2 molecules per square cavity. Iodine atoms of the two molecules in the cavity are 4.13 Å apart which is slightly longer than the separation in solid I_2 of 3.97 Å.[13] Of particular importance is the close contact that is made between the iodine atoms and the carbon atoms of the chloranilate that are bound to chlorine atoms (Fig. 3). The separation between the carbon and iodine atoms is 3.33 Å, which is significantly less than the sum of the van der Waals radii for carbon and iodine of 3.68 Å.[12] The interaction between the iodine molecules and the host network causes the bridging chloranilate ligand to tilt towards the iodine molecule. In the parent network the Cl···Cl vector of a single chloranilate ligand is inclined at an angle of 23° to the direction of the channels whereas in the crystal containing iodine the angle is decreased to 14°. Furthermore, the C···C separation across the channel decreases from 9.71 Å in the acetone solvate (9.86 Å in the desolvated crystal) to 9.30 Å in the I_2 compound.

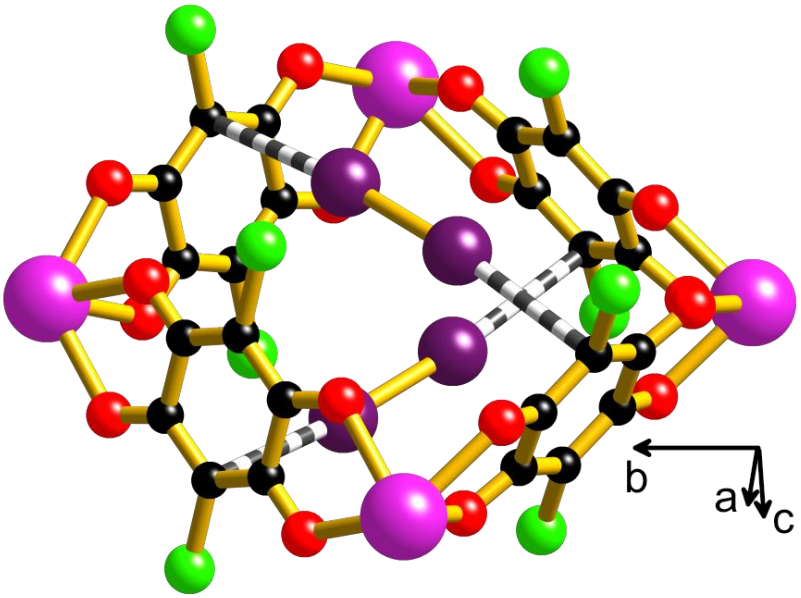

Figure 3. A square cavity within the $[Y(can)_2]^-$ framework, occupied by I_2 molecules (deep purple). The site occupancy for each I_2 molecule refined to ~95%, indicating that both orientations are occupied in the majority of cavities. The striped connections represent I···C interactions (3.33 Å)

$(Et_4N)[Y(can)_2]\cdot 0.9(Br_2)$

Single crystals of the desolvated $(Et_4N)[Y(can)_2]$ were placed in a capped vial containing a smaller open vial which held a drop of liquid Br_2. Over a period of a day the bromine vapor was allowed to diffuse into the $(Et_4N)[Y(can)_2]$ crystals. Single crystal X-ray analysis revealed retention of the host network and the incorporation of Br_2 molecules in the square cavities of the $[Y(can)_2]^-$ network (see Figure 4). Although the Br_2 was disordered, it was possible to identify discrete Br_2 molecules and the site occupancy of each molecule was refined. Refinement of the structure revealed that 91(1) % of the square cavities were singly occupied by a Br_2 molecule; the remaining sites are empty. As was the case with the iodine, a bromine atom makes close contact with the carbon bound to the chloranilate Cl atom (3.25 Å)

which is less than the sum of the van der Waals radii for carbon and bromine (3.55 Å).[12] Unlike iodine, the bromine molecule is not long enough to span the C···C separation across the channel.

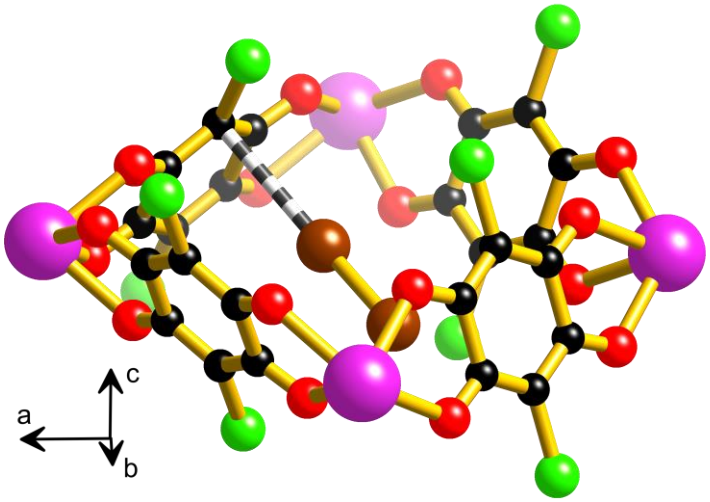

Figure 4. A square cavity within the $[Y(can)_2]^-$ framework $(Et_4N)[Y(can)_2]\cdot 0.9(Br_2)$ occupied by a disordered Br_2 molecule (brown). Shown is one of eight symmetry-equivalent orientations. Close contact of one of the Br atoms with the C of the chloranilate ligand (3.25 Å) is indicated by a striped connection.

Gas adsorption studies

In preparation for gas uptake measurements the host network was activated by heating a sample of $(Et_4N)[Y(can)_2]$ to 200 °C under vacuum. Using a manometric technique, isotherms were recorded for the uptake of hydrogen and nitrogen at both 77 and 87 K. Similarly, isotherms measured at 258, 273 and 298 K were recorded for methane and carbon dioxide. All isotherms exhibit a type I shape.[14] Adsorption isotherms for H_2, CH_4 and CO_2 are presented in Figure 5. Adsorption isotherms collected at different temperatures are presented in Figures S2.1 and S2.2 (Supporting Information). A summary of the gas sorption results including calculations of binding enthalpies at initial loading is presented in Table 2. The results indicate not only significant uptake of gases but also relatively high binding enthalpies for each of the gases. For example, the binding enthalpy for methane of 28.5 kJ mol^{-1} is amongst the highest for porous coordination polymers.[15] Similarly, the adsorption binding enthalpies for H_2, N_2 and CO_2 are

high relative to other coordination polymer systems.[16] In the absence of direct interaction with metal centres, the high adsorption enthalpies probably reflect the interaction with multiple surfaces in the crystal pores.

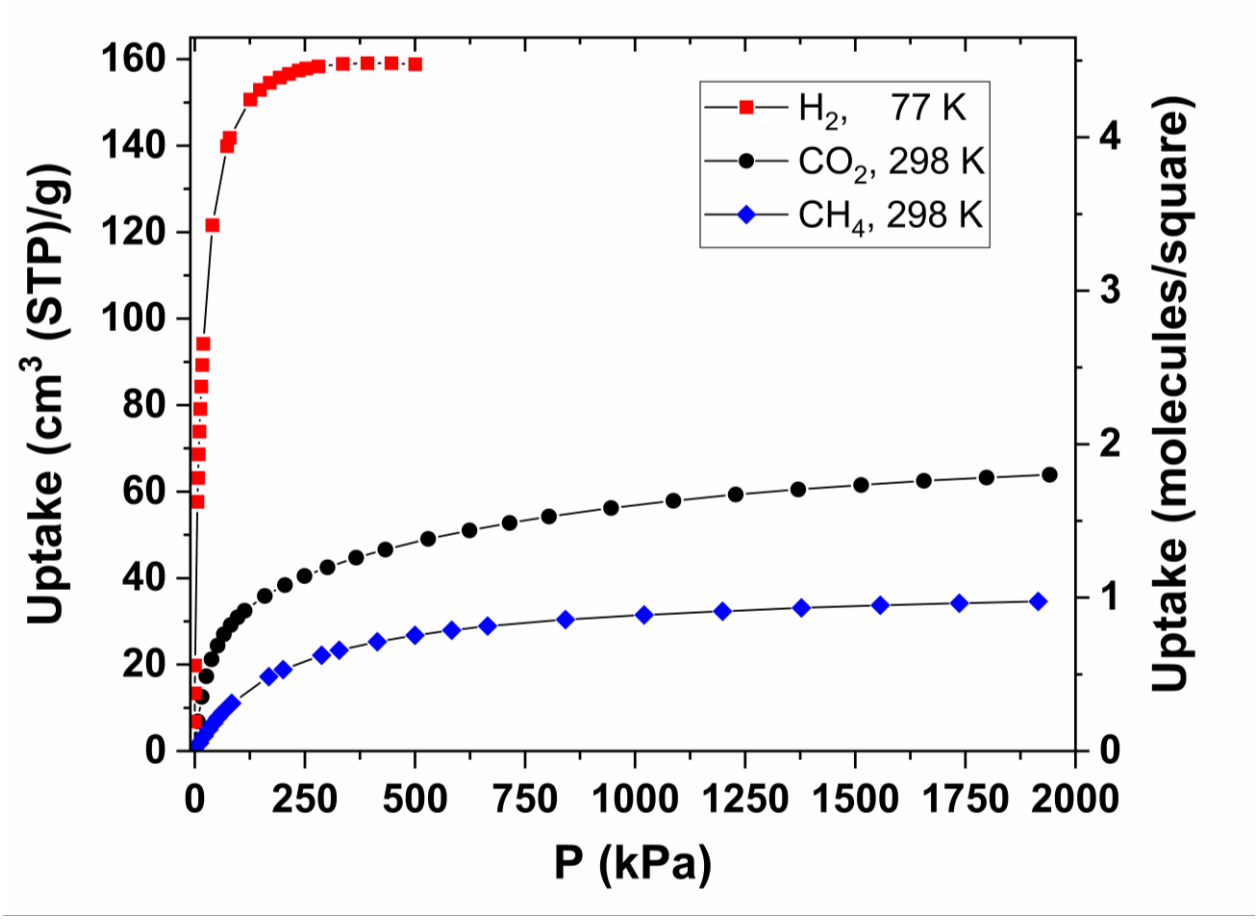

Figure 5. Adsorption isotherms recorded for the uptake of hydrogen, carbon dioxide and methane by the host network, $(Et_4N)[Y(can)_2]$.

Table 2. Selected gas adsorption data for activated $(Et_4N)[Y(can)_2]$

Compound	**Gas**	***T***	***P*** *	**Uptake** †			**-Δ*H*$_{ads}$** §
		(K)	*(kPa)*	*(cm^3/g)*	*(mg/g)*	*(n/M)*	*(kJ/mol)*
$(Et_4N)[Y(can)_2]$	H_2	77	190	158	14	4.4	9.6
	N_2	77	25	164	202	4.6	25.0
	CH_4	258	3070	44	31	1.2	28.7
	CO_2	258	1850	86	167	2.4	38.6

* Pressure at which the uptake values were measured corresponding to the maximum uptake indicated by the isotherm.

† Uptake expressed in: cm^3 (at STP)/g, mg (of gas)/g (host material) and no. of guest molecules per Y center.

§ Isosteric heat of adsorption at initial loading. For H_2 and N_2 the values were calculated from isotherms measured at 77 and 87 K, for CH_4 and CO_2 the values were calculated from isotherms measured at 258, 273 and 298 K.

***In situ* neutron powder diffraction-gas adsorption experiments on $Et_4N[Y(can)_2]$**

In order to obtain a better understanding of the interactions between square grid coordination polymers and intercalated gases, a microcrystalline sample of $Et_4N[Y(can)_2]$ was investigated in a series of *in situ* neutron powder diffraction (NPD) experiments performed in conjunction with quantitative adsorption of D_2 (D = deuterium), CD_4, and CO_2. The use of deuterated gases was necessary to limit excessive background signal due to the large incoherent neutron scattering cross-section of ^1H. Gas dosing was achieved using a manometric apparatus described in the Supporting Information S3.

The positions of the adsorbed gas molecules were initially determined by dosing the sample with known quantities of gas and cooling to 15 K to minimise thermal atomic motion. Fourier difference maps obtained from Rietveld refinements against data collected under these conditions revealed nuclear density in the pores of $(Et_4N)[Y(can)_2]$ unaccounted for by the host structure, which was attributed to the positions of guest gas molecules (see following sections). Analysis of these data also revealed that the incorporation of guest molecules exerts only a minor effect on the cell parameters, with the largest observed increase in unit cell volume being ~0.7% observed at a sample loading of 1.5 CO_2 molecules per metal center.

Additional *in situ* NPD data were collected at 3 min intervals during gas adsorption isotherms recorded at 258 K (CO_2, CD_4) and 77 K (D_2). These isotherms are in good agreement with those reported in the previous section (see Figure S2.3, Supporting Information). Sequential Rietveld refinements allowed the fractional guest occupancies at the various identified sites to be quantified as a function of guest concentration.

CO_2

Nuclear density consistent with CO_2 guests was apparent at two positions; the dominant position, observed in both the high-intensity NPD data at 258 K and the high-resolution data at 15 K, was similar to the location of the CS_2 molecules in the single crystal X-ray structural analysis (see Figure 2a). The location of residual nuclear density at 15 K after dosing with 0.5, 1.0 and 1.5 molecules of CO_2 per metal center is depicted in Figure 6. The site occupancy refined to 0.78(2) at the final (highest loading) point of the adsorption isotherm, corresponding to 1.56(4) molecules of CO_2 per Y center, with considerable

positional disorder evident in the nuclear density obtained by Fourier difference methods obtained from the high-resolution data at a loading of 1.5 CO_2 molecules per metal center (Figure 6c). A second binding site was also observed at high CO_2 loadings in the 258 K isotherm data set only, and was located in the same plane as the Et_4N^+ cations which lie between the anionic sheets (see supporting information, Figure S3.3). The refined occupancy of this secondary site resulted in an additional 0.161(16) CO_2 molecules per Y center at the maximum recorded isothermal CO_2 loading, for a total of 1.72(10) CO_2 molecules per Y center identified at crystallographically ordered sites in $Et_4N[Y(can)_2]$.

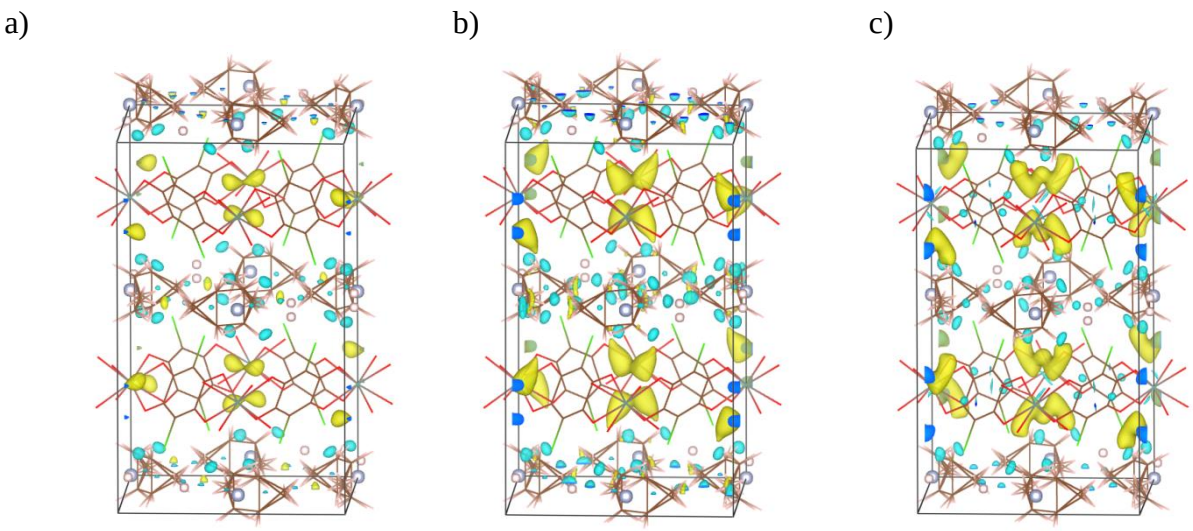

Figure 6. Representations of residual nuclear density in $(Et_4N)[Y(can)_2]$ at 15 K after dosing with a) 0.5, b) 1.0, and c) 1.5 eq. CO_2. Yellow and light blue features indicate positive and negative residual nuclear density, respectively, between +/-0.09 fm/Å^3. Bonds between framework atoms are represented as coloured lines (atoms are omitted for clarity). The crystallographic *c* axis is vertical.

D_2

At low loadings in the high-resolution NPD experiment, D_2 was found to occupy a site (site 1) corresponding to the center of the square hole in the anionic $[Y(can)_2]^-$ network (Figure 7a). This site is bounded by the faces of the four surrounding chloranilate ligands. As the loading increased towards one D_2 per Y centre, a second binding site (site 2) was observed in the plane of the cation layer. Above this loading, site 1 gradually became unoccupied and a third binding site (site 3) appeared, effectively corresponding to the splitting of site 1 into 4 equivalent lobes which approach the faces of the chloranilate

ligands. Site 1 and site 2 are separated by a distance of 5.1 Å which corresponds to ¼ of the *c* axis. Site 3 is located 2.25 Å from site 1 and 3.69 Å from site 2.

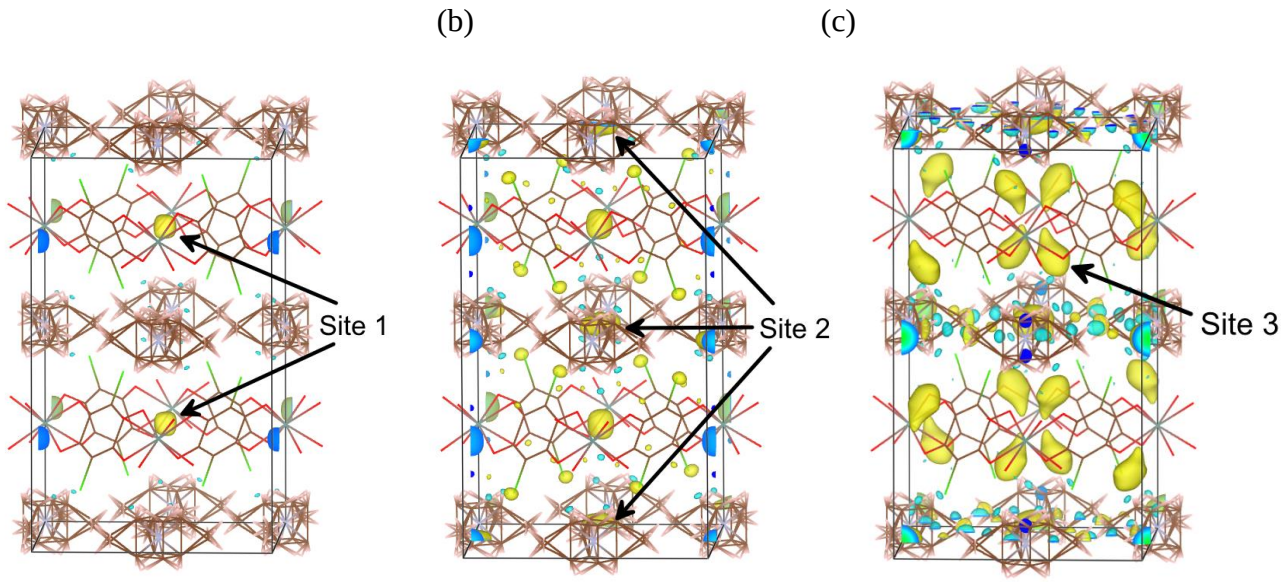

Figure 7. Representations of residual nuclear density in $(Et_4N)[Y(can)_2]$ dosed with a) 0.5, b) 1.0, and c) 3.0 D_2 molecules per Y center. Yellow and light blue features indicate positive and negative residual nuclear density, respectively, between +/-0.1 fm/Å^3. Bonds between framework atoms are represented as coloured lines (atoms are omitted for clarity). The crystallographic *c* axis is vertical. Site 1 is located in the plane of the $Y(can)_2]^-$ and is apparent in (a) and (b); site 2 lies in the plane of the NEt_4^+ cations and is located in the middle of the top and bottom faces and also in the center of the unit cell; only one of the site 3 positions in (c) is indicated.

This progressive three-site D_2 loading model is well supported by the results of density functional theory (DFT)-based molecular dynamics (MD) simulations, which were performed for a unit cell of $Et_4N[Y(can)_2]$ containing different concentrations of D_2 guest molecules at 70 K. Trajectories of the guest molecules can be used to create frequency distribution maps of guest molecules which show guest occupancy in the structure. 25 ps calculation results show localised D_2 residing at site 2 and considerable occupancy distributed over sites 1 and 3 at a loading of 3 D_2 molecules per Y center, whereas site 1 is not substantially occupied. The "splitting" of site 1 into the four lobes of site 3 is observed more distinctly at a loading of 5 D_2 molecules per Y center. (Figure 8).

(a) (b)

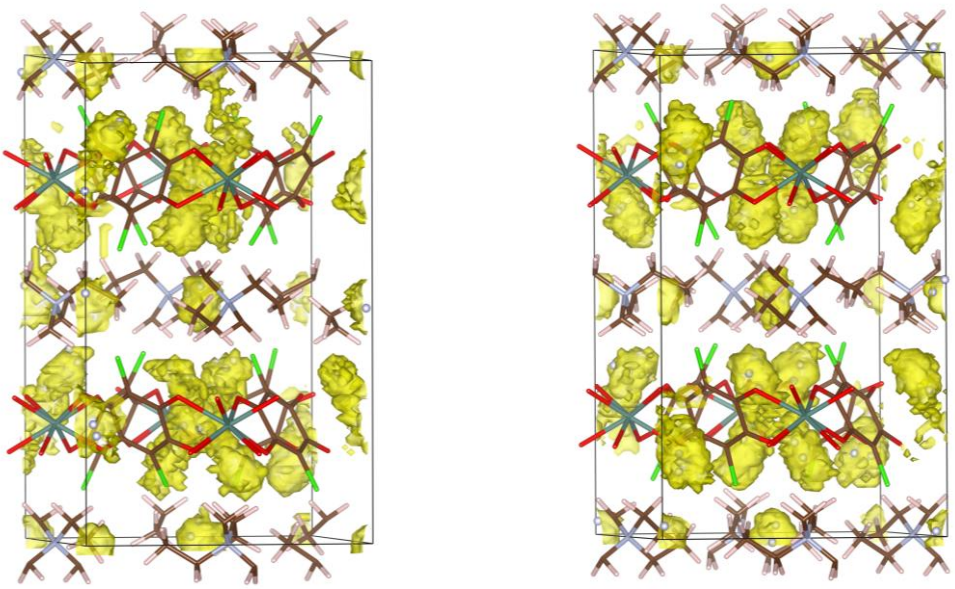

Figure 8. Integrated guest occupancy maps (yellow surfaces) illustrating the frequency distribution of D_2 guest molecules over the course of ~28 ps DFT-MD simulations at 70 K, at guest concentrations of (a) 3 and (b) 5 per Y centre.

The maximum recorded uptake of 4.91 D_2 per Y centre achieved during the *in situ* adsorption isotherm measurement, which appeared to end slightly before saturation, is consistent with the expected occupancy of 5 D_2 molecules per Y center if sites 2 and 3 are fully loaded. Site occupancy trends obtained by refinement against the isothermal NPD data series also agreed well with the findings of the high-resolution study, except that the filling of site 3 commenced at the lowest loadings and increased continuously over the whole D_2 concentration range (Figure 9). We speculate that at the slightly higher temperatures used during the isothermal NPD experiment, the D_2 molecules are able to move between the closely neighboring sites 1 and 3, leading to co-filling of both of these sites until the increased concentration renders the low-capacity site 1 unfavorable. Indeed, the MD frequency distribution plot obtained for a loading of 3 D_2 molecules per Y at 70 K (Figure 8a) illustrates the relative ease with which D_2 guests can move between sites 1 and 3, while transfers between these sites and site 2 in the cation layer do not occur over the timescale of the simulation (~28 ps).

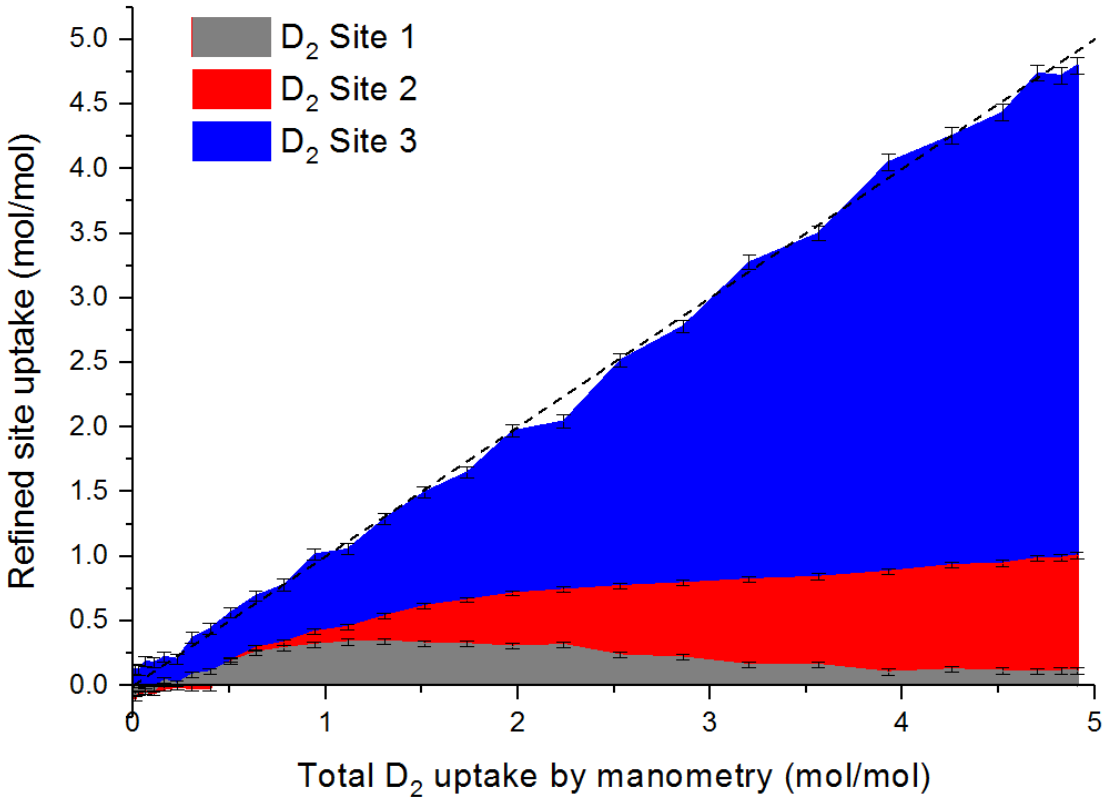

Figure 9. Site-specific D_2 loadings calculated from fractional occupancies refined against *in situ* NPD data for $Et_4N[Y(can)_2]$ and plotted as a function of the total D_2 uptake (as determined by the volumetric dosing system). The dashed line represents a 1:1 ratio between the dosed and total refined loading amounts. No constraints were applied to the refined site occupancies.

CD_4

Although high-resolution NPD data were not available for the CD_4-dosed framework, Fourier difference methods using the last NPD pattern in the CD_4 adsorption isotherm dataset clearly revealed residual nuclear density only at the centre of the square holes of the anionic layer, in a comparable location to the initial site (site 1) that was occupied by D_2 (Figure 10). On the basis of the unit cell symmetry and the somewhat isotropic form of the Fourier difference peak, the adsorbed methane molecule was considered to be rotationally averaged and was modelled accordingly as a single C atom with a large isotropic atomic displacement factor and "fractional occupancy" allowed to exceed 1. The refined occupancy of the residual nuclear density arising from CD_4 at the highest loading in the isotherm NPD dataset, corresponded to the nuclear scattering from 0.857(17) CD_4 molecules per Y centre, comparable with the final recorded volumetric uptake of 1.0 CD_4 per Y center.

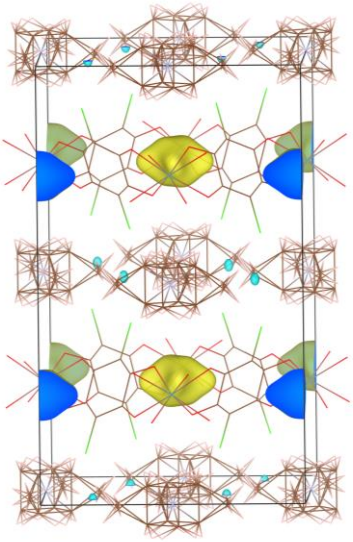

Figure 10. Representation of residual nuclear density in $(Et_4N)[Y(can)_2]$ after cumulative isothermal doses of CD_4 up to a total of 1.0 per Y centre. Yellow and very light blue features indicate positive and negative residual nuclear density, respectively, between +/-0.07 fm/Å^3.

It is interesting to consider the significance of the NPD study of the methane loaded system in the context of the high isosteric heat of adsorption value calculated from the isotherms described earlier (see Figure 5 and Table 2). The site occupied by the methane molecule lies at the centre of the square cavity and the distance from this site to the centres of the four surrounding chloranilate ligands is approximately 4.3 Å. Allowing for a van der Waals "thickness" of 3.4 Å for the chloranilate ligand, the separation between the centre of the cavity and the van der Waals surface of the anionic network is 2.6 Å [4.3 - (3.4/2)]. Given that the estimated van der Waals radius of methane is ~2.3 Å, it is clear that the square cavity is a good fit for the methane molecule, and this would seem to be a feasible explanation for the high binding enthalpy.[17]

Magnetic susceptibility studies on $(Et_4N)[M^{III}(can)_2]$ (M =Gd, Dy)

The magnetic properties of chloranilate-bridged framework materials are currently of great interest[3d, 5b-d, 18] not only for those containing diamagnetic can^{2-} bridges but also, particularly, those containing radical can^{3-} bridges of the semiquinone type found in d-block anilato families such as $[Fe_2(can)_3]^{2-}$, the latter forming a 6,3- hexagonal network structure.[5a, 5c] The present 2D 4,4-network is an attractive system to explore magnetic properties, including magnetic exchange, as each Ln(III) centre is bridged by four can^{2-} groups to neighbouring Ln(III) centres. The paramagnetic lanthanide ions, however, show much weaker exchange coupling than their *d*-ion congenors, and some of them display large magnetic anisotropy that can potentially lead to slow magnetisation reversal effects. From the present $(Et_4N)[M^{III}(can)_2]$ family we chose one orbitally non-degenerate ion, Gd^{III}, and one orbitally degenerate ion, Dy^{III} for investigation for magnetic susceptibility.

The $\chi_M T$ vs. temperature plot for $(Et_4N)[Gd^{III}(can)_2]$ is shown in Figure 11(a) under two DC applied fields which indicate little or no field dependence except at very low temperatures. The crystalline sample had been desolvated by heating *in vacuo*, for 2 h at 90 °C, prior to loading in to the gel capsule container and then into the sample chamber of the Squid magnetometer. The $\chi_M T$ values remain independent of temperature between 300 and ~20 K, at 7.4 $cm^3\ mol^{-1}$ K, then decrease rapidly down to 2 K, reaching 5 $cm^3\ mol^{-1}$ K, due to zero field splitting combined possibly with weak antiferromagnetic exchange. The uncoupled free ion value for $f^7(^8S_{7/2})$ Gd^{III} is 7.86 $cm^3\ mol^{-1}$ K, a little higher than observed. The *M* vs *H* isotherms are shown in Figure 11(b), in fields of 0 – 5 T at temperatures 2 to 20 K. Saturation is almost achieved at 2 K and 5 T, the value of *M* being 6.4 $N\mu_B$, a little lower than the spin only value of 7 $N\mu_B$. The magnetic behaviour is essentially single ion with little evidence for exchange coupling being of any significance. When *M* is plotted against *H*/temperature, at 2, 3, 4 and 5.5 K, the lines all lie on a single curve indicative of very small anisotropy (i.e. zero field splitting near zero); see Supporting Information Figure S6.1.

a)

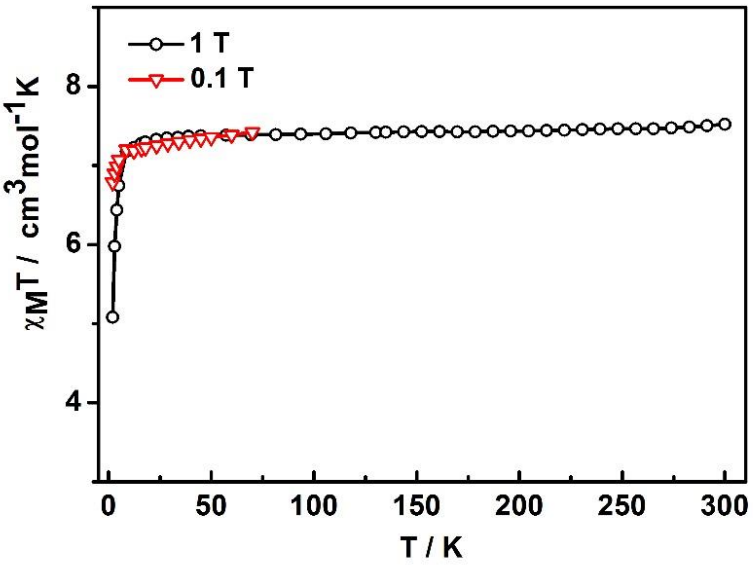

b)

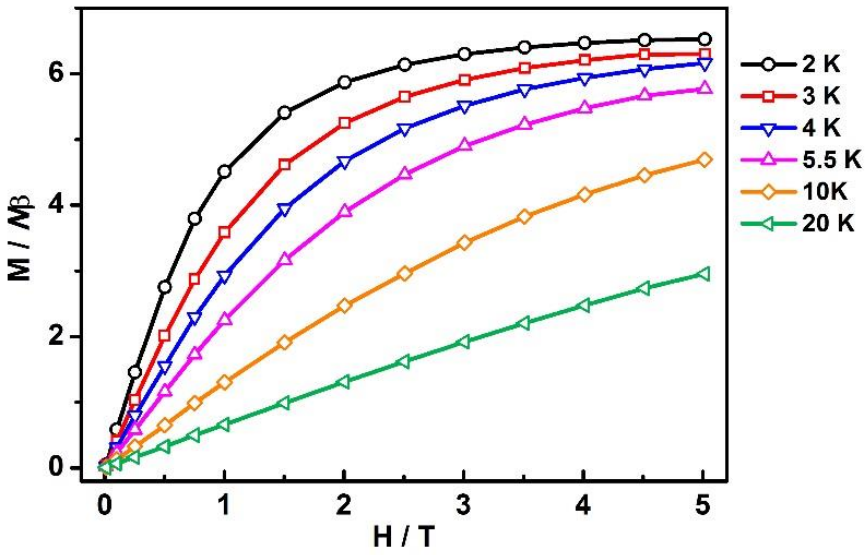

Figure 11. Plots of a) $\chi_M T$ vs T (top) and b) M vs H isotherms for $(Et_4N)[Gd^{III}(can)_2]$

The DC magnetic data for $(Et_4N)[Dy^{III}(can)_2]$ are shown in Figure 12. There is a small field dependence in $\chi_M T$ between 70 and 2 K in fields of 0.1 and 1 T. The room temperature value in the 1 T field is 13.8 cm^3 mol^{-1} K, in quite good agreement with the free ion value of 14. 17 cm^3 mol^{-1} K for an f^9 ($^6H_{15/2}$) system. This difference might be due to partial desolvation of the sample, trace magnetic impurities or intrinsic antiferromagnetic exchange coupling. On lowering the temperature, a slow

decrease occurs down to ~50 K, with a $\chi_M T$ value of 4.5 cm^3 mol^{-1} K reached, more rapidly, at 2 K. The overall decrease is suggestive of depopulation of single ion Dy^{III} m_J sub-levels of the ground J multiplet combined, perhaps, with weak antiferromagnetic coupling.

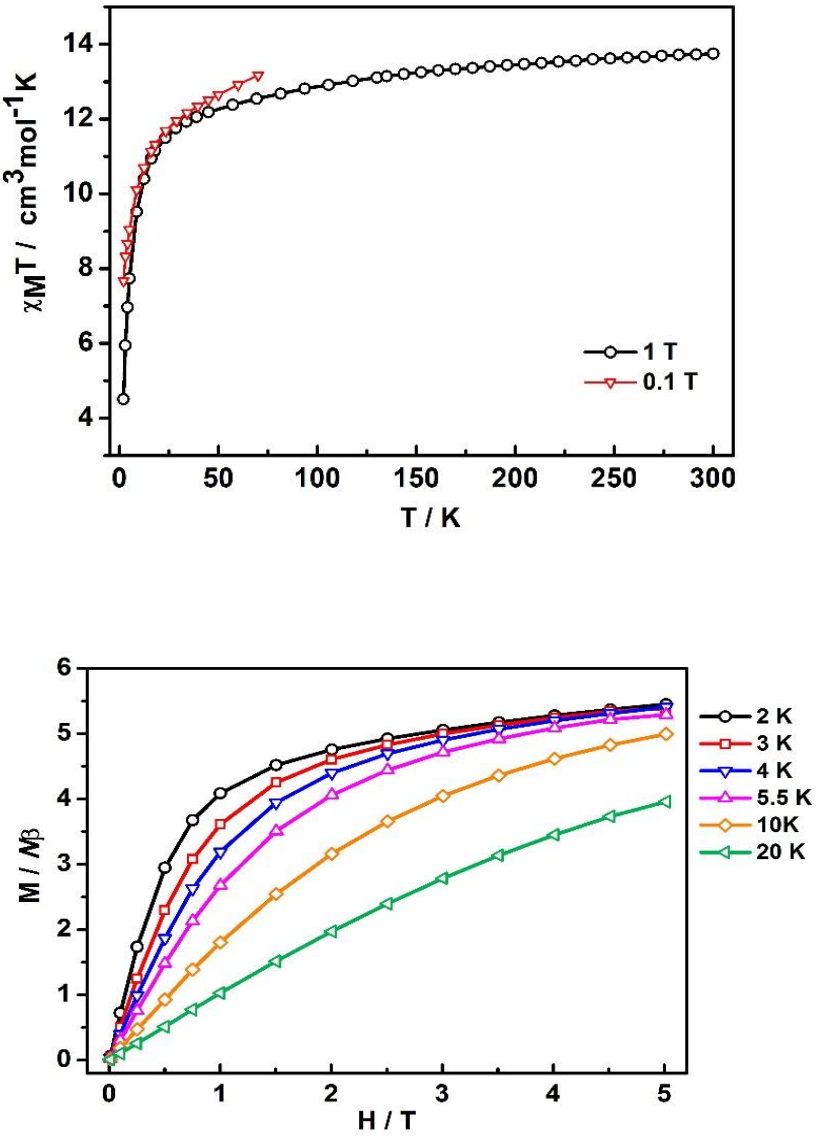

Figure 12 Plots of a) $\chi_M T$ vs T and b) M vs H isotherms for $(Et_4N)[Dy^{III}(can)_2]$

The magnetisation isotherms, shown in Figure 12, are typical of Dy^{III} complexes[19] with the 2-4 K plots not reaching saturation and tending to overlap above H = 3 T on account of low lying Zeeman levels being close together. The 2 K/5 T magnetisation value is lower than the expected saturation value for a Dy^{III} ion as a result of crystal-field effects eliminating the 16-fold degeneracy of the $^6H_{15/2}$ ground state and the effects of low-lying excited states.

AC susceptibility measurements were made to detect any slow magnetic relaxation effects in these Ln^{III} framework species. The in-phase (χ_M') and out-of-phase (χ_M″) susceptibility data, measured between 2 and 10 K in AC frequencies 0 – 1488 Hz, and in a DC fields of 0 T and 0.1 T for Dy and 0 T and 0.35 T for Gd, are shown in the Supporting Information, Figures S6.2 to S6.7. The Dy example shows no temperature dependence of χ_M″ in zero DC field but shows frequency dependent 'tails' below 3 K in the 0.1 T DC field with no clear maxima, suggestive of slow magnetisation reversal occurring. An unusual peak occurs at 7 K in higher AC frequencies perhaps suggestive of a long range ordered trace impurity. The χ_M' data show Curie-like behaviour with no frequency dependence between 2 and 10 K.

Intriguing AC results were noted for $(Et_4N)[Gd^{III}(can)_2]$ since this isotropic f^7 ion as a free ion would normally be expected to show no frequency dependent χ_M″ behaviour. In zero DC field the χ_M″ values are zero and independent of frequency, apart for the 1488 Hz plot becoming a little negative below 4 K (Figure S6.4). In Figure S6.7, it can be seen that broad, frequency dependent maxima are observed in a DC field of 0.35 T at 3 K (997 Hz) and 4 K (1488 Hz), while frequency dependent tails are observed for lower frequencies. There is precedence for such behaviour in the case of a chain structure found in the complex $Na[Gd(EDTA)(H_2O)_3]\cdot 5H_2O$.[20] The zig-zag chains are made up of doubly water/η_1-carboxylate bridged -$(O)_2$-Gd-$(O)_2$-Na-$(O)_2$-Gd- moieties with the intramolecular distance between Gd··Gd ions being 6.0782(5) Å. Dipolar Gd···Gd interactions were deemed to be important in the magnetism rather than superexchange interactions. The Gd···Gd separation in the present network is 8.66368(14) Å, across the can^{2-} bridges. The slow relaxation of magnetisation in the EDTA species, observed in a 0.45 T DC field, was ascribed to spin phonon transitions between the closely spaced levels (< 1 cm^{-1}) brought about by spin-orbit splitting of the ground ^8S ground state, the latter yielding anisotropy. However, it has been shown that distortions of the crystal field in polyoxometallate single-ion compounds of type $[Gd(W_5O_{18})_2]^{9-}$ lead to anisotropy and slow magnetisation relaxation occurring in the milliKelvin range.[21] Hence it is not clear which mechanism appears likely to apply to $(Et_4N)[Gd^{III}(can)_2]$ but other anilate network solids need to be investigated, along with theoretical (*ab initio* and DFT) calculations to confirm this and to see how widespread slow relaxation is for Gd^{III} species. We have preliminary observations for similar frequency dependent AC behaviour in DC fields for lanthanide networks such as

$(NBu_4)_2[Gd_2(can)_5(Na(H_2O)_3)_2]$ with maxima in χ_M'' being clearly observed.[22] We also note that slow magnetisation relaxation has recently been reported for the 2D transition metal network material $(NPr_4)_2[Fe_2(can)_3].2acetone.H_2O$.[23]

Conclusion

The original motivation for this work stemmed from our investigations of a previously reported compound, $(NEt_4)_2[Sn^{IV}Ca^{II}(can)_4]$ and our interest in determining if a large +3 metal cation could fulfil the role of the 8-coordinate Sn(IV) and Ca(II) ions in related structures. This current work has clearly demonstrated that the porous square grid network is not limited to a single compound but in fact, $(NEt_4)_2[Sn^{IV}Ca^{II}(can)_4]$ is part of a large family of porous materials consisting of parallel square grid $[M(an)_2]^-$ (an = anilate) networks in which M may be one of the following metals: Sc, Y, Gd, Tb, Dy, Ho, Er, Yb, Lu, In or Bi. Furthermore, the bridging ligand within the anionic network was found not to be limited to chloranilate with both bromoanilate and chlorocyanoanilate each yielding similar structures. The tetraalkylammonium cation, mainly NEt_4^+, plays a similar structural role in each compound, located between metal centres of adjacent sheets.

Investigation of the host properties of representative compounds, in particular $(NEt_4)_2[Y(can)_2]$, have clearly shown the ability of the network materials to adsorb appropriately sized guest molecules such as H_2, CH_4, N_2, CO_2, CS_2, Br_2 and I_2 with the location of the guest molecules indicated by single crystal X-ray diffraction or neutron powder diffraction. High adsorption enthalpies recorded for H_2, N_2, CO_2 and particularly CH_4 are likely to reflect the ability of these molecules to simultaneously interact with more than one internal surface of the square channel.

Finally, the magnetic properties of $(Et_4N)[Gd^{III}(can)_2]$ and $(Et_4N)[Dy^{III}(can)_2]$ showed magnetic data typical of these single ions, possibly with weak coupling, as well as unusual slow magnetisation dynamics in the Gd(III) case that deserves further investigation in framework species of this f^7 ion.

Experimental

Synthesis

H_4can was synthesised according to a literature method.[24] H_4ClCNan was prepared by a similar procedure from K_2ClCNan·H_2O, which was prepared by the procedure of Atzori *et al.*[5f] H_4Bran was prepared from H_2Bran by a similar procedure, which was prepared by the procedure of Stenhouse.[25]

$(Et_4N)[Y(can)_2]\cdot(CH_3)_2CO$

A solution of H_4can (1.0 mmol, 0.21 g) and LiOAc (2.0 mmol, 0.13 g) in acetone (20 ml) was layered above $Y^{III}(NO_3)_3\cdot 6H_2O$ (0.50 mmol, 0.19 g) and Et_4NBr (2.0 mmol, 0.42 g) in water (10 mL). This solution was left to stand in a partially covered flask and crystals appeared at the interface between the two solutions within two days. After one week, large block-like, dark purple crystals were filtered from the solution and washed with water and acetone. X-ray powder diffraction data (see Supporting Information) indicated that the bulk product possessed the same structure as the single crystal used in the structure determination. Elemental analysis, calcd (%) for $(Et_4N)[Y(can)_2]$ C 37.9, H 3.2, N 2.2; found C 37.3, H 3.3, N 2.2; Yield 0.187 g, 54%.

$(Et_4N)[M^{III}(can)_2]\cdot x(CH_3)_2CO$ (M = Sc, In, Gd, Tb, Dy, Ho, Er, Yb, Lu, Bi $1 \leq x \leq 2$)

A solution of H_4can (0.10 mmol, 0.021 g) and LiOAc (0.20 mmol, 0.013 g) in acetone (5 ml) was layered above $M^{III}(NO_3)_3\cdot x(H_2O)$ (M = Sc, Tb, Ho, Er, Yb, Lu, Bi, 0.050 mmol) and Et_4NBr (0.50 mmol 0.11 g) in water (3mL). This mixture was left to stand in a partially covered flask, and crystals appeared at the interface between the two solutions within two days. After three days, large, block-like, dark purple crystals, for all compounds except for $(Et_4N)[Bi^{III}(can)_2]$ which were red, were filtered from the solution, and washed with water and acetone.

For all of these compounds X-ray powder diffraction data of the bulk product was described well by the single crystal determined structure. Elemental analysis, calcd (%) for $(Et_4N)[Sc(can)_2]$ C 40.8, H 3.4, N 2.4; found C 41.6, H 4.0, N 2.3. Yield for $(Et_4N)[M(can)_2]$: M = Sc 0.0141 g, 44%; Tb 0.0095 g, 24%; Ho 0.0156 g, 39%; Er 0.0162 g, 42%; Yb 0.0142 g; 37%, Lu 0.0101 g, 25%; Bi 0.0297 g, 71%.

$(Et_4N)[Bi^{III}(can)_2]\cdot 2(CH_3)_2CO$ was dark red; otherwise, the precipitates were uniformly dark purple.

$(Et_4N)[M^{III}(can)_2]\cdot x(CH_3)_2CO$ (M = In, Gd, Dy; $1 \leq x \leq 1.5$)

Microcrystalline samples of the compounds $(Et_4N)[M^{III}(can)_2]$ (M = Dy, Gd, In) could be formed by mixing the components at high-temperature, and showed powder diffraction patterns consistent with the single crystal structure. Single crystals of the above compounds were formed by layering processes described for $(Et_4N)[Y^{III}(can)_2]$.

H_2can (0.20 mmol, 0.042 g) was combined with $M^{III}(NO_3)_3$ (M = Gd, Dy) or $M^{III}Cl_3$ (M = In) (0.10 mmol) in 10 ml water and 30 ml acetone containing Et_4NBr (1.0 mmol) and LiOAc (0.40 mmol) was added to the solution, and the resulting purple precipitate was stirred at reflux for two hours. On cooling, the purple precipitate was filtered and washed with water until filtrate was colourless (approx. 2 x 5 ml), then 10 ml acetone, and dried at the pump. For all of these compounds, powder X-ray diffraction data of the bulk product were well described by the single crystal determined structure. Yield M = Gd 0.0446 g, 59%; Dy 0.0224 g, 28%; In 0.0321 g, 43%.

$(Me_4N)[Sc(can)_2]\cdot((CH_3)_2CO)$

A solution of 1.0 mmol of H_4can and 2.0 mmol of LiOAc in acetone (20 ml) was layered above 0.50 mmol of $Sc^{III}(NO_3)_3\cdot 6H_2O$ and 2.0 mmol of Et_4NBr in water (10mL). This solution was left to stand in a partially covered flask, and crystals appeared at the interface between the two solutions within two days. After one week, large, block-like dark purple crystals were filtered from the solution, and washed with water and acetone. Calcd (%) for $(Me_4N)[Sc(can)_2]$ C 36.0, H 2.3, N 2.6; found C 35.7, H 2.3, N 2.6; Yield 0.251g, 94%.

$(Et_4N)[Bi(Bran)_2]\cdot 1.5(CH_3)_2CO$

A solution of 0.10 mmol of H_2Bran in acetone (20 ml) was layered above 0.050 mmol of $Bi^{III}(NO_3)_3\cdot 6H_2O$ and 0.30 M Et_4NBr solution in water (3 mL). This solution was left to stand in a partially covered flask, and crystals appeared at the interface between the two solutions within two days. After one week, square plate, dark red crystals appeared within a flocculant colourless precipitate, presumably bismuth oxynitrate. Crystals could be isolated by filtering over a coarse frit, and washed with water and acetone. Yield 0.0336 g, yield 66%.

$(Et_4N)[Bi(ClCNan)_2]\cdot 1.5((CH_3)_2CO)$

A solution of 0.10 mmol of $K_2ClCNan$ in acetone/water (15ml) was layered above 0.05 mmol $Bi^{III}(NO_3)_3 \cdot 6(H_2O)$ and 0.30 M Et_4NBr solution in water (3mL). This solution was left to stand in a partially covered flask and crystals appeared at the interface between the two solutions within two days. After one week, square plate dark red crystals appeared within a flocculant colourless precipitate, presumably bismuth oxynitrate; crystals could be isolated by filtering over a coarse frit, and washed with water and acetone. Yield 0.022 g, 54%.

Inclusion of CS_2, I_2 and Br_2 into $(Et_4N)[Y(can)_2]$

A sample of $(Et_4N)[Y(can)_2]$ was heated to 110°C overnight under vacuum in a tube furnace to ensure the channels in the structure were empty. This compound was used as the starting material for the inclusion experiments involving the guests CS_2, I_2 and Br_2. Single crystals of $(Et_4N)[Y(can)_2] \cdot 1.43(CS_2)$ were obtained by immersing the activated $(Et_4N)[Y(can)_2]$ in liquid CS_2 for 24 hours at room temperature in a capped vial, and transferred directly to a protective oil before being mounted on a single crystal diffractometer. In the case of $(Et_4N)[Y(can)_2] \cdot 1.87(I_2)$, the inclusion of iodine occurred by adsorption of iodine vapor. Single crystals of desolvated $(Et_4N)[Y(can)_2]$ (approx. 1 mg) were placed in a capped vial containing solid I_2 (one large crystal, approx. 50 mg) for two days at room temperature. A crystal was then transferred directly to protective oil and mounted on a single crystal diffractometer. A similar process was employed in the generation of $(Et_4N)[Y(can)_2] \cdot 0.91Br_2$ with single crystals of $(Et_4N)[Y(can)_2]$ placed in a capped vial containing a second smaller vial which contained one drop of liquid bromine. After 24 hours exposure to the Br_2 vapor a crystal was transferred directly to protective oil and mounted on a single crystal diffractometer.

Single crystal structure determination

Single crystals were analysed on an Oxford Diffraction Supernova diffractometer with CuKα microfocus radiation (λ = 1.5418 Å), with samples held at 130.0(1) K except where otherwise indicated. Data collection, reduction and absorption corrections were all performed within using the program CrysAlisPro.[26] Absorption corrections were performed, using either numerical[27] or empirical methods.[27, 28]

Structures were solved using SHELXT,[29] and refined using the full matrix least-squares model on F^2 with SHELXL.[30] Each structure exhibited disorder of the tetraalkylammonium cation over two symmetry-related orientations. Additional details regarding single crystal structure determination are presented in the Supporting Information (S1). Crystallographic tables relating to these compounds are presented in Table S1.1.

X-ray Powder Diffraction

X-ray powder diffraction data for $(Et_4N)[Ho^{III}(can)_2]\cdot 1.5(CH_3)_2CO$; $(Et_4N)[Er^{III}(can)_2]\cdot(CH_3)_2CO$; $(Et_4N)[Sc^{III}(can)_2]\cdot(CH_3)_2CO$; $(Et_4N)[Lu^{III}(can)_2]\cdot 1.5(CH_3)_2CO$; $(Et_4N)[Tb^{III}(can)_2]\cdot 1.5(CH_3)_2CO$; $(Et_4N)[Yb^{III}(can)_2]\cdot(CH_3)_2CO$ were collected using synchrotron radiation at 0.7907(10) Å. Powder diffraction data for $(Et_4N)[Y(can)_2]\cdot(CH_3)_2CO$, $(Et_4N)[Bi(ClCNan)_2]\cdot 1.5(CH_3)_2CO$ and $(Et_4N)[Bi(Bran)_2]\cdot 1.5(CH_3)_2CO$ were collected using synchrotron radiation at 0.7745(10) Å. Powder diffraction data for $(Et_4N)[Gd^{III}(can)_2]\cdot 1.5(CH_3)_2CO$, $(Et_4N)[Dy^{III}(can)_2]\cdot 1.5(CH_3)_2CO$, $(Et_4N)[Bi^{III}(can)_2]\cdot 2(CH_3)_2CO$, $(Me_4N)[Sc^{III}(can)_2]\cdot(CH_3)_2CO$ were collected using CuKα radiation at 1.5418 Å.

Synchrotron X-ray powder diffraction data were collected on the powder diffraction beamline at the Australian Synchrotron. The samples were loaded into Lindemann glass capillary tubes as slurries in acetone and mounted on the powder diffraction beamline. The wavelengths were refined from a NIST SRM 660b LaB_6 standard reference material. Data were collected using the Mythen microstrip detector from 3 – 83° 2θ. To cover the gaps between detector modules, 2 datasets were collected with the detector set 0.5° apart and then merged to a single dataset.

Laboratory based X-ray powder diffraction data were collected using a CuKα source on an Oxford Diffraction Supernova diffractometer. Samples were loaded as powder into Lindemann glass capillary tubes and patterns were collected at 130 K.

X-ray powder diffraction data are presented in the Supporting Information (S4), where patterns are also calculated from the structures determined by single crystal X-ray diffraction.

Gas Sorption

Gas uptake was measured by differential pressure using a Sievert-type BELsorp-HP automatic gas sorption apparatus (BEL Japan Inc.). Ultra-high purity CO_2, CH_4, N_2 and H_2 gases were purchased from BOC and Air Liquide. Samples were prepared by desolvation under dynamic vacuum at elevated temperature (200 °C) and reactivated at this temperature under vacuum between measurements. Full description of the gas adsorption procedure is provided in the supporting information.

Gas Sorption-Powder Neutron Diffraction

In situ neutron powder diffraction (NPD) data were collected using the high-intensity powder diffractometer WOMBAT[31] and the high-resolution diffractometer ECHIDNA[32] at the OPAL reactor, ANSTO, Australia. All measurements were performed on samples of $Et_4N[Y(can)_2]$ with a known mass which were dried by heating under vacuum at 200 °C and transferred to a sealed vanadium can inside a helium-filled glove box. The sample can was attached to a custom-designed gas delivery sample stick[33] and positioned inside a helium cryofurnace, keeping the sample isolated from air. A Hiden Isochema IMI manometric dosing system was used to conduct fully computer-controlled gas dosing experiments and maintain sample temperature control throughout the NPD experiments.

High-resolution NPD data were obtained at 15 K for activated $(Et_4N)[Y(can)_2]$ and for discrete loadings of D_2 (0.5, 1.0, 2.0 and 3.0 per Y center) and CO_2 (0.5, 1.0 and 1.5 per Y center). NPD data were collected on ECHIDNA with a neutron wavelength of 2.4395 Å, using a 2θ step size of 0.05° in the range $6.5 \leq 2\theta \leq 165°$.

High-intensity NPD data were collected for continuously and recorded at 3 min intervals during isothermal adsorption of CO_2, CD_4 and D_2.[34] The neutron wavelength $\lambda = 2.95314(11)$ Å was refined using data for the NIST 660b LaB_6 standard reference material and data were collected in the range $13.5 \leq 2\theta \leq 133°$.

Rietveld refinements against NPD data were performed using the GSAS-II program.[35] The structure of the empty $Et_4N[Y(can)_2]$ framework, based on the single crystal structure of the solvated $Et_4N[Y(can)_2]\cdot(CH_3)_2CO$ was first refined against a high-resolution NPD data recorded at 15 K. Details

of the collected data and the refinements are presented in the Supporting Information, alongside examples of Rietveld refinement profiles and agreement indices.

Magnetism studies

A Quantum Design MPMS 7 magnetometer was used to measure DC and AC susceptibilities and magnetisations. Polycrystalline samples of mass ~25 mg were contained in a calibrated gel capsule that was held at the centre of a drinking straw which was fixed to the end of the sample rod. In the case of anisotropic $(Et_4N)[Dy(can)_2]$, a Vaseline mull of the sample was employed to eliminate any anomalous torquing effects. Prior to placing the samples in the capsule the samples were heated in a vacuum at 90 °C for 2 hours to remove any solvent molecules from the crystal lattice.

Acknowledgements

We thank the Australian Research Council for support through the Discovery Project scheme. This research is supported by the Science and Industry Endowment Fund. Part of this research was undertaken on the PD beamline at the Australian Synchrotron, part of ANSTO. We acknowledge the support of the Australian Centre for Neutron Scattering, Australian Nuclear Science and Technology Organisation, in providing the neutron research facilities used in this work.

Supporting Information

CCDC 1824739-1824755 and 1829220 contain the supporting crystallographic information for this paper. These data are provided free of charge by The Cambridge Crystallographic Data Centre. Supporting Information contains details of single crystal structure determinations (S1), gas sorption (S2), neutron powder diffraction (S3), X-ray powder diffraction (S4), density finctional theory molecular dynamics simulations (S5), magnetism (S6) and themogravimetic analysis (S7).

References

[1] a) R. W. Gable, B. F. Hoskins, R. Robson, *J. Chem. Soc., Chem. Commun.* **1990**, 1677-1678; b) F. Robinson, M. J. Zaworotko, *J. Chem. Soc., Chem. Commun.* **1995**, 2413-2414; c) S. Subramanian, M. J. Zaworotko, *Angew. Chem. Int. Ed.* **1995**, *34*, 2127-2129; d) L. R. MacGillivray, S. Subramanian, M. J. Zaworotko, *J. Chem. Soc., Chem. Commun.* **1994**, 1325-1326; e) O. M. Yaghi, H. Li, *J. Am.Chem. Soc.* **1995**, *117*, 10401-10402; f) O. M. Yaghi, G. Li, *Angew. Chem. Int. Ed.***1995**, *34*, 207-209; g) O. M. Yaghi, H. Li, *J. Am.Chem. Soc.* **1996**, *118*, 295-296; h) P. Losier, M. J. Zaworotko, *Angew. Chem. Int. Ed.* **1996**, *35*, 2779-2782; i) M. Fujita, Y. J. Kwon, S. Washizu, K. Ogura, *J. Am.Chem. Soc.* **1994**, *116*, 1151-1152.

[2] S. Kitagawa, S. Kawata, *Coord. Chem. Rev.* **2002**, *224*, 11-34.

[3] a) B. F. Abrahams, T. A. Hudson, L. J. McCormick, R. Robson, *Cryst. Growth Des.* **2011**, *11*, 2717-2720; b) B. F. Abrahams, A. M. Bond, T. H. Le, L. J. McCormick, A. Nafady, R. Robson, N. Vo, *Chem. Commun.* **2012**, *48*, 11422-11424; c) M. E. Ziebel, L. E. Darago, J. R. Long, *J. Am.Chem. Soc.* **2018**, *140*, 3040-3051; d) L. E. Darago, M. L. Aubrey, C. J. Yu, M. I. Gonzalez, J. R. Long, *J. Am.Chem. Soc.* **2015**, *137*, 15703-15711.

[4] A. Weiss, E. Riegler, C. Robl, *Z. Naturforsch. B* **1986**, *41b*, 1501-1505.

[5] a) C. J. Kingsbury, B. F. Abrahams, D. M. D'Alessandro, T. A. Hudson, R. Murase, R. Robson, K. F. White, *Cryst. Growth Des.* **2017**, *17*, 1465-1470; b) I.-R. Jeon, B. Negru, R. P. Van Duyne, T. D. Harris, *J. Am.Chem. Soc.* **2015**, *137*, 15699-15702; c) J. A. DeGayner, I.-R. Jeon, L. Sun, M. Dincă, T. D. Harris, *J. Am.Chem. Soc.* **2017**, *139*, 4175-4184; d) R. Murase, B. F. Abrahams, D. M. D'Alessandro, C. G. Davies, T. A. Hudson, G. N. L. Jameson, B. Moubaraki, K. S. Murray, R. Robson, A. L. Sutton, *Inorg. Chem.* **2017**, *56*, 9025-9035; e) S. Benmansour, A. Hernández-Paredes, C. J. Gómez-García, *J. Coord. Chem.* **2018**, *71*, 845-863; f) M. Atzori, S. Benmansour, G. Mínguez Espallargas, M. Clemente-León, A. Abhervé, P. Gómez-Claramunt, E. Coronado, F. Artizzu, E. Sessini, P. Deplano, A. Serpe, M. L. Mercuri, C. J. Gómez García, *Inorg. Chem.* **2013**, *52*, 10031-10040; g) N. S. Ovanesyan, Z. K. Nikitina, V. D. Makhaev, *Bull. Russ. Acad. Sci.: Phys.* **2017**, *81*, 855-859; h) A. Abhervé, M. Clemente-León, E. Coronado, C. J. Gómez-García, M. Verneret, *Inorg. Chem.* **2014**, *53*, 12014-12026; i) M. Palacios-Corella, A. Fernández-Espejo, M. Bazaga-García, E. R. Losilla, A. Cabeza, M. Clemente-León, E. Coronado, *Inorg. Chem.* **2017**, *56*, 13865-13877.

[6] S. Halis, A. K. Inge, N. Dehning, T. Weyrich, H. Reinsch, N. Stock, *Inorg. Chem.* **2016**, *55*, 7425-7431.

[7] B. F. Abrahams, M. J. Grannas, T. A. Hudson, S. A. Hughes, N. H. Pranoto, R. Robson, *Dalton Trans.* **2011**, *40*, 12242-12247.

[8] a) B. F. Abrahams, J. Coleiro, B. F. Hoskins, R. Robson, *Chem. Commun.* **1996**, 603-604; b) B. F. Abrahams, J. Coleiro, K. Ha, B. F. Hoskins, S. D. Orchard, R. Robson, *Journal of the Chemical Society, Dalton Trans.* **2002**, 1586-1594.

[9] P. Gómez-Claramunt, S. Benmansour, A. Hernández-Paredes, C. Cerezo-Navarrete, C. Rodríguez-Fernández, J. Canet-Ferrer, A. Cantarero, J. C. Gómez-García, *Magnetochem.* **2018**, *4*.

[10] B. F. Abrahams, A. D. Dharma, B. Dyett, T. A. Hudson, H. Maynard-Casely, C. J. Kingsbury, L. J. McCormick, R. Robson, A. L. Sutton, K. F. White, *Dalton Trans.* **2016**, *45*, 1339-1344.

[11] A. L. Spek *Acta Crystallogr.* **2009**, *D65*, 148-155.

[12] a) A. Bondi, *J . Phys. Chem.*, **1964**, 68, 441-451 b) R. S. Rowland, R. Taylor, *J. Phys. Chem.* **1996**, *100*, 7384-7391.

[13] F. van Bolhuis, P. B. Koster, T. Migchelsen, *Acta Cryst.* **1967**, *23*, 90-91

[14] K. S. W. Sing, *International Union of Pure and Applied Chemistry* **1982**, *54*, 2210-2218.

[15] a) K. Konstas, T. Osl, Y. Yang, M. Batten, N. Burke, A. J. Hill, M. R. Hill, *J. Mater. Chem.* **2012**, *22*, 16698-16708; b) Y. Peng, V. Krungleviciute, I. Eryazici, J. T. Hupp, O. K. Farha, T. Yildirim, *J. Am.Chem. Soc.* **2013**, *135*, 11887-11894; c) T. A. Makal, J.-R. Li, W. Lu, H.-C. Zhou, *Chem. Soc. Rev.* **2012**, *41*, 7761-7779; d) K. F. White, B. F. Abrahams, R. Babarao, A. D. Dharma, T. A. Hudson, H. E. Maynard-Casely, R. Robson, *Chem. Eur. J.* **2015**, *21*, 18057-18061; e) Y. He, W. Zhou, G. Qian, B. Chen, *Chem. Soc. Rev.* **2014**, *43*, 5657-5678.

[16] a) H. Furukawa, N. Ko, Y. B. Go, N. Aratani, S. B. Choi, E. Choi, A. Ö. Yazaydin, R. Q. Snurr, M. O'Keeffe, J. Kim, O. M. Yaghi, *Science* **2010**, *329*, 424; b) Z. R. Herm, J. A. Swisher, B. Smit,

R. Krishna, J. R. Long, *J. Am.Chem. Soc.* **2011**, *133*, 5664-5667; c) B. Mu, P. M. Schoenecker, K. S. Walton, *J. Phys. Chem. C* **2010**, *114*, 6464-6471; d) A. R. Millward, O. M. Yaghi, *J. Am.Chem. Soc.* **2005**, *127*, 17998-17999.

[17] H. Wu, J. M. Simmons, Y. Liu, C. M. Brown, X.-S. Wang, S. Ma, V. K. Peterson, P. D. Southon, C. J. Kepert, H.-C. Zhou, T. Yildirim, W. Zhou, *Chem. Eur. J.* **2010**, *16*, 5205-5214.

[18] M. L. Mercuri, F. Congiu, G. Concas, S. A. Sahadevan, *Magnetochem.* **2017**, *3*.

[19] S. K. Langley, N. F. Chilton, B. Moubaraki, K. S. Murray, *Inorg. Chem.* **2013**, *52*, 7183-7192.

[20] R. J. Holmberg, L. T. A. Ho, L. Ungur, I. Korobkov, L. F. Chibotaru, M. Murugesu, *Dalton Trans.* **2015**, *44*, 20321-20325.

[21] M. J. Martinez-Pérez, S. Cardona-Serra, C. Schlegel, F. Moro, P. J. Alonso, H. Prima-García, J. M. Clemente-Juan, M. Evangelisti, A. Gaita-Ariño, J. Sesé, J. van Slageren, E. Coronado, F. Luis, *Phys. Rev. Lett.* **2012**, *108*, 247213.

[22] K. S. Murray, W. Phonsri, *Unpublished data* **2018**.

[23] J. Chen, Y. Sekine, Y. Komatsumaru, S. Hayami, H. Miyasaka, *Angew. Chem. Int. Ed.* **2018,** *57*, 12043-12047

[24] P. R. Weider, L. S. Hegedus, H. Asada, S. V. D'Andreq, *J. Org. Chem.* **1985**, *50*, 4276-4281.

[25] J. Stenhouse, *J. Chem. Soc.* **1870**, *23*, 6-14.

[26] CrysAlisPRO, *Oxford Diffraction /Agilent Technologies UK Ltd*, ***2017***.

[27] R. C. Clark, J. S. Reid, *Acta Crystallographica Section A* **1995**, *51*, 887-897.

[28] R. H. Blessing, *Acta Crystallogr. Sect. A* **1995**, *51*, 33-38.

[29] G. M. Sheldrick, *Acta Crystallogr. Sect. A* **2015**, *71*, 3-8

[30] G. M. Sheldrick, *Acta Crystallogr. Sect. C* **2015**, *71*, 3-8.

[31] A. J. Studer, M. E. Hagen, T. J. Noakes, *Physica B: Cond. Matter* **2006**, *385-386*, 1013-1015.

[32] K.-D. Liss, B. Hunter, M. Hagen, T. Noakes, S. Kennedy, *Physica B: Condens. Matter* **2006**, *385-386*, 1010-1012.

[33] a) S. Lee, H. Chevreau, N. Booth, S. G. Duyker, S. H. Ogilvie, P. Imperia, V. K. Peterson, *J. Appl. Crystallogr.* **2016**, *49*, 705-711; b) H. Chevreau, S. G. Duyker, V. K. Peterson, *Acta Crystallogr. Sect. B* **2015**, *71*, 648-660.

[34] J. E. Auckett, S. G. Duyker, D. R. Turner, S. R. Batten, V. K. Peterson, *ChemPlusChem* **2018**, *83*, 669-675.

[35] B. H. Toby, R. B. Von Dreele, *J. Appl. Crystallogr.* **2013**, *46*, 544-549.

Author/s:
Kingsbury, CJ; Abrahams, BF; Auckett, JE; Chevreau, H; Dharma, AD; Duyker, S; He, Q; Hua, C; Hudson, TA; Murray, KS; Phonsri, W; Peterson, VK; Robson, R; White, KF

Title:
Square Grid Metal-Chloranilate Networks as Robust Host Systems for Guest Sorption

Date:
2019-04-05

Citation:
Kingsbury, C. J., Abrahams, B. F., Auckett, J. E., Chevreau, H., Dharma, A. D., Duyker, S., He, Q., Hua, C., Hudson, T. A., Murray, K. S., Phonsri, W., Peterson, V. K., Robson, R. & White, K. F. (2019). Square Grid Metal-Chloranilate Networks as Robust Host Systems for Guest Sorption. CHEMISTRY-A EUROPEAN JOURNAL, 25 (20), pp.5222-5234. https://doi.org/10.1002/chem.201805600.